Int. J. Electrochem. Sci., 17 **(2022)** Article Number: 220410, doi: 10.20964/2022.04.57

International Journal of
ELECTROCHEMICAL
SCIENCE
www.electrochemsci.org

Synthesis and Anodic Performances of Hard-carbon Microspheres for Sodium and Lithium Ion Capacitors

Wanxing Sheng[1,], Qing Duan[1,*], Dandan zhao[2], Guanglin Sha[1], Yunzhao Wu[1,*], Yao Zhang[1], Weichao Zhang[1], Yi Mu[1], Jian Gao[1], Chunyan Ma[1], Haili Lin[1]*

[1] China Electric Power Research Institute, No.15 Xiaoying East Road, Qinghe, Beijing 100192, China
[2] Kunshan Kunpeng Lijie NANO Polymer Co. Ltd., Kunshan, Jiangsu 215300, China
[*]E-mail: wxsheng@epri.sgcc.com.cn, duanqing@epri.sgcc.com.cn, wuyunzhao@epri.sgcc.com.cn

Received: 9 December 2021 / *Accepted:* 10 January 2022 / *Published:* 4 March 2022

Hard-carbon microspheres were synthesized in this study by a microemulsion-mediated hydrothermal method, and hard-carbon powder was prepared by a normal hydrothermal method for comparison. The BET results indicated that the electrode material obtained from the hard-carbon microsphere had narrow particle size distribution and uniform dispersion. The hard-carbon microspheres had more micropore structures than mesopore structures. The electrical conductivity, rate performance, and specific capacitance of the hard-carbon microsphere as anode materials in sodium ion capacitors were better than the hard-carbon powder. In terms of their future application, the hard-carbon microsphere materials could be used for high energy and power density Na-ion and Li-ion capacitors with low cost and safety.

Keywords: Hard carbon; Microsphere; Micropore; Anode; Capacitor; Micromulsion

1. INTRODUCTION

Carbon materials are generally used as anode for sodium and lithium-ion capacitors owe to their low-cost and relative high ion storage capacity [1-3]. The graphite-type materials are still not good enough to meet the requirements for the batteries ascribe to its low theoretical specific capacity (372 mAh/g) [4]. Hard carbon has drawn much attention attribute to its high reversible specific capacity, generally 500-700 mAh/g [5-8]. Hard Carbon refers to hard graphitized carbon, which is usually the thermal decomposition product of polymer [9]. Their stable structure, long charge-discharge cycle life, and good rate performance of hard carbon can satisfy the requirements for high-power ion batteries [10-12]. Besides, hard carbon is more compatible with electrolytes than graphite-type materials. In addition to the potential application as anode material for ion capacitors, it also possesses attractive prospect applied as the support material for Pt catalyst for direct methanol fuel cells [13].

In recent years, many new hard carbon materials have been reported [14-21]. It is discovered that the micropore structure plays a significant role in the ion insertion and extraction process due to ionic thermodynamic and kinetic behaviors [22-24]. Larger micropores show better kinetic performance at high current density while smaller micropores lead to higher thermodynamic ion-storage voltage which is beneficial for achieving higher ion-insertion capacity [19]. Water-in-oil microemulsion method has been applied to synthesize nanomaterials with narrow particle size distribution. A water-in-oil microemulsion is a thermodynamically stable, optically isotropic, and transparent solution stabilized by surfactant [25, 26]. The aqueous phase is dispersed in the continuous oil phase as microdroplets surrounded by a monolayer of surfactant molecules [27]. In this study, hard-carbon microspheres were synthesized by a microemulsion-mediated hydrothermal method, and hard-carbon powder was prepared by a normal hydrothermal method for comparison. They show different microstructures, which lead to different electrochemical performance as anode materials in ion capacitors. It indicates that we should design hard carbon materials with different micropore structures for different application purposes.

2. EXPERIMENTAL

2.1. Preparation of hard-carbon materials

Formaldehyde (F, 37 wt% aqueous solution) and resorcinol (R) were employed as dispersed aqueous phase (A). The molar ratio of R:F was 1:2. The mixture of F and R was stirred at 900r/min for 60mins, and then the obtained A was left standing for 12h. Sodium dodecyl sulfate (SDS) was used as the surfactant (S), and silicon oil was applied as continuous oil phase (O). The weight ratio of S:A:O was 1:100:10000. Microemulsion was prepared by dispersing S and A into O through intense stirring. The viscosity of the mixed solution was 200mPa·s, and the stirring rate was 400r/min at room temperature. The reaction system was then heated at constant temperature of 120℃ for 30mins. After forming the microspheres, oxalic acid (Ac) was added. The molar ratio of S:Ac was 1:1. After constant temperature reaction at 120℃ for 60mins, the microspheres were filtered out of the silicone oil. The microspheres were repeatedly washed by hot water for 3 times, and then placed in an oven to dry at 100℃ to obtain the resin microsphere precursor. The precursors of resin microspheres were placed in a muffle furnace under protection of nitrogen atmosphere, heated to 1000ºC and held for 3h to obtain hard carbon microspheres.

The hard-carbon powder was prepared through a normal two-step procedure: hydrothermal at a low temperature and then carbonized at a high temperature [28]. The above-mentioned A with sodium carbonate (C) as a catalyst was added into a 100 mL hydrothermal reactor and heated at 120 ℃ for 12 h. The molar ratio of R:F and R:C were 1:2 and 200:1, respectively. The obtained powder was washed by distilled water and dried at 100 ℃ for 24 h. Then the powder was further pyrolyzed for 3h in a muffle furnace at 1000 ℃ in a nitrogen atmosphere. All the reagents (A.R.) were commercial products (Sigma Aldrich).

2.2. Characterization of hard-carbon materials

The morphology of the sample was investigated by a field emission scanning electron microscope (FESEM, a Hitachi S-4800). The structure of the sample was characterized by X-ray diffraction (Rigaku D/MAX 2400 diffractometer, Cu Kα radiation) and infrared spectrometer (IR, NEXUS 670). The nitrogen adsorption/de-adsorption isotherms were performed on a BET surface area and pore size analyzer (ASAP2020M & TriStar3020). Before BET measurement, samples were vacuumed for 12 h at 350℃.

2.3. Electrochemical measurements of hard-carbon materials

The electrochemical properties of hard-carbon as anode materials in sodium ion capacitors were investigated by using a three-electrode electrochemical cell containing 0.5 M Na_2SO_4 aqueous electrolyte [29]. The freshly prepared hard-carbon electrode was used as working electrode, with a platinum foil (area 1 cm^2) as counter electrode, and an Ag/AgCl electrode as reference electrode. The hard-carbon electrode was prepared by mixing hard-carbon (85 wt.%), acetylene black (10 wt.%) and polytetrafluoroethylene (PTFE) (5 wt.%). The mass of active materials was about 5 mg. A small amount of distilled water was added to the mixtures to make them more homogeneous. The mixtures were pressed onto nickel foam current collectors (1.0×1.0 cm^2) to fabricate electrodes. After that, the as-prepared electrode was dried under vacuum at 120 ℃ for 12 h.

The electrochemical properties of the hard-carbon samples were also investigated by using a Li/hard-carbon button-type lithium ion battery. The composite electrode was prepared by mixing hard-carbon (80 wt.%), acetylene black (10 wt.%) and polyvinylidene fluoride (PVDF) (10 wt.%) in N-methyl pyrrolidone. The slurry of active material was spread onto a copper foil with a surface density of 8 mg/cm^2. The sheet was dried under vacuum at 120 ℃ for 12 h and then cut into small electrode sheets (1.2 cm^2). Li foil was applied as counter electrode, and 1 M $LiPF_6$ dissolved in a mixture of ethylene carbonate (EC) and dimethyl carbonate (DMC) (1:1 by volume) was used as the electrolyte. Test cells were assembled in an argon-filled glove box.

For each experiment, the test cell was rested for 24 h to approach the equilibrium state. Cyclic voltammetry (CV), galvanostatic charge–discharge (GCD) tests, and electrochemical impedance spectroscopy (EIS) were conducted by an electrochemical workstation (CHI660E). The test cells were discharged to 0 V and the open-circuit voltage was measured. EIS was performed at the open circuit potential. Data were collected in the frequency range of 10^5 to 10^{-2} Hz. All of the electrochemical measurements were carried out at room temperature.

3. RESULTS AND DISCUSSION

3.1. Morphology and structure of hard-carbon microspheres

Fig. 1 compares the morphologies of the two kinds of hard-carbon materials. The hard-carbon microsphere material showed perfect spherule shape and narrow particle size distribution (Fig. 1a and

1b). This may have benefited from the microemulsion mediated hydrothermal method [28]. The average sphere diameter for the hard-carbon microspheres sample was about 15–65 μm. The hard-carbon electrode material obtained by smashing hard-carbon microspheres had narrow particle size distribution and uniform dispersion (Fig. 1c). In contrast, the hard-carbon powder (Fig. 1d) was severely aggregated with irregular shape.

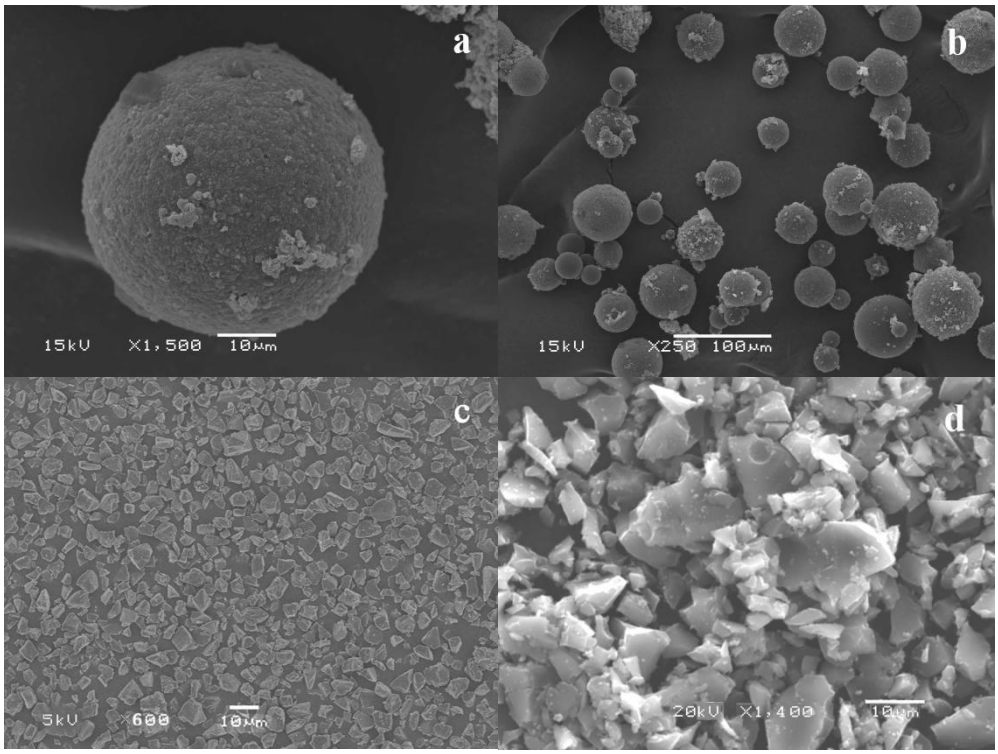

Figure 1. SEM images of (a) and (b) the hard-carbon microspheres; (c) the hard-carbon electrode material obtained by smashing the hard-carbon microspheres; and (d) the hard-carbon powder.

XRD patterns of (a) the hard-carbon microsphere and (b) the hard-carbon powder were compared in Fig. 2. The XRD data for the hard-carbon microsphere and hard-carbon powder is also listed in Table 1. They showed typical disordered-carbon structure [28]. Meanwhile, their diffraction intensities were very strong at low Bragg angles, indicating a porous feature of these materials based on the Bragg law. These two samples showed multi-peaks patterns and their peak-widths were broad, which indicated that the pore size distributions (PSD) of these two samples were not uniform [28].

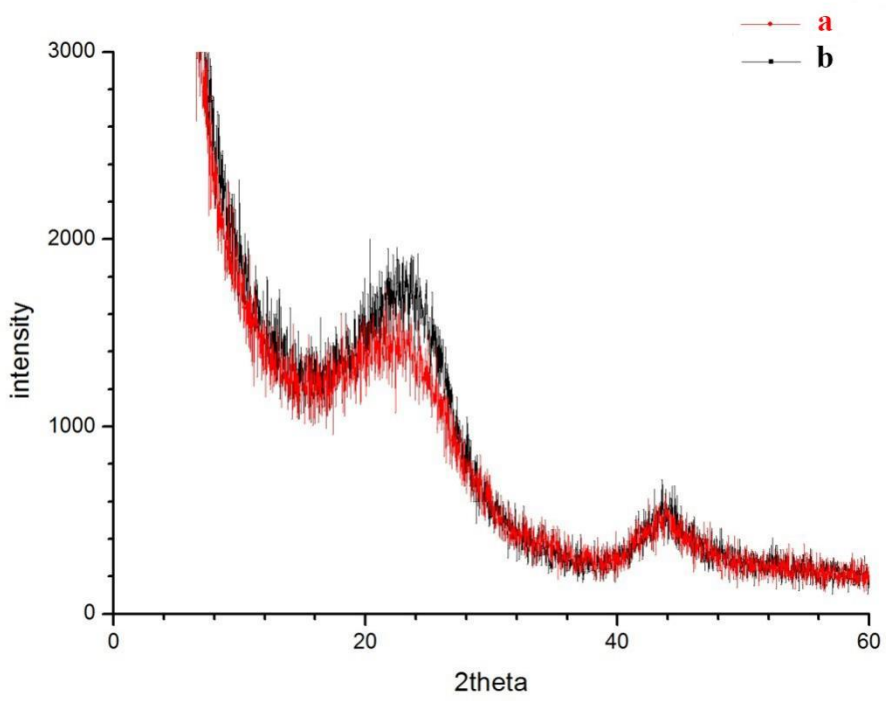

Figure 2. XRD patterns of (a) the hard-carbon microspheres (red line) and (b) the hard-carbon powder (black line).

Table 1. XRD data of the hard-carbon microspheres (red line a in Figure2) and the hard-carbon powder (black line b in Fig.2).

Samples	2theta	Flex Width	d-value	Intensity	I/I_0
Hard-carbon microspheres	23.300	0.165	3.8145	1450	100
Hard-carbon powder	23.240	0.235	3.8243	1767	100

The Infrared spectrograms of these two kinds of hard-carbon samples are shown in Fig. 3. In Fig. 3a, the peaks at 2961.10 cm^{-1} and 2924.59 cm^{-1} represented methyl and methylene groups. In addition, the peaks at 1449.50 cm^{-1}, 879.61 cm^{-1}, 636.75 cm^{-1}, and 515.08 cm^{-1} indicated the presence of carbonates. The comparison between Fig. 3a and Fig. 3b showed that the surface of the hard-carbon microsphere sample was rich in alkyl groups, hydroxyl groups, and possibly carbonates. These groups and substances may be introduced by the preparation process of hard-carbon microspheres. It is confirmed that the alkyl groups can be converted into peroxides or alcohols conducing to intermolecular cross-linkage [30].

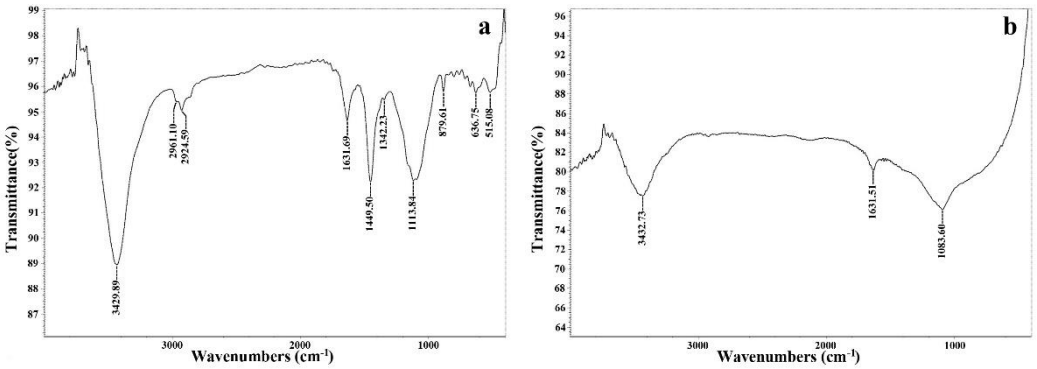

Figure 3. IR spectrograms of (a) the hard-carbon microspheres and (b) the hard-carbon powder.

The micropore structures of the carbon materials were investigated by the adsorption/desorption isotherms based on BET model. The nitrogen adsorption/desorption isotherm curves and the corresponding pore size distribution (PSD) of the Hard-carbon microspheres are shown in Fig. 4. The N_2 adsorption isotherm for the Hard-carbon microspheres (Fig. 4a) are typical of type I in the Brunauer-Deming-Deming-Teller (BDDT) classification, indicating that the Hard-carbon microspheres were typical microporous materials [28]. The mesoporous hysteresis ring for the nitrogen adsorption/desorption isotherm curve belonged to H4 model, which often occurs in solids containing narrow fissure pores and slot pores mixed with micropores and mesopores. It can be seen clearly from the corresponding mesopore PSD curve by BJH model (Fig. 4b) and the micropore PSD curve by HK model (Fig. 4c) that the Hard-carbon microspheres have more micropore structures than mesopore structures.

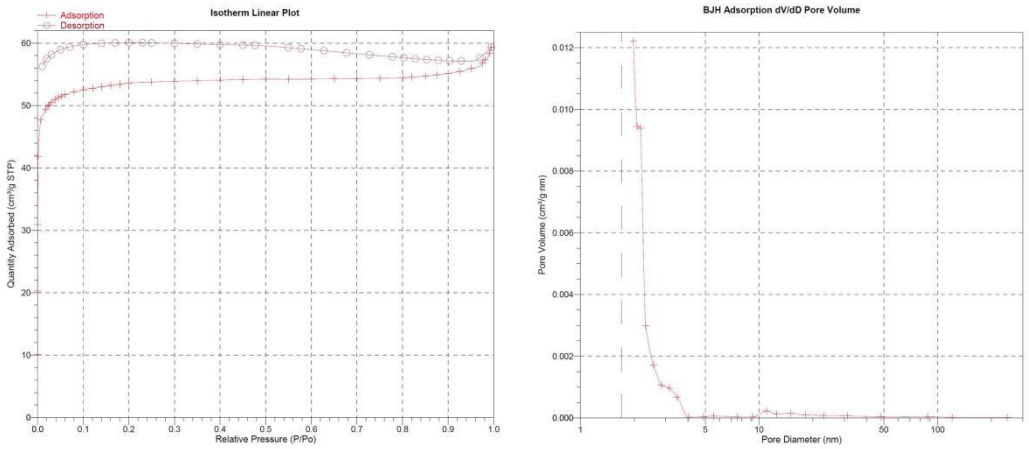

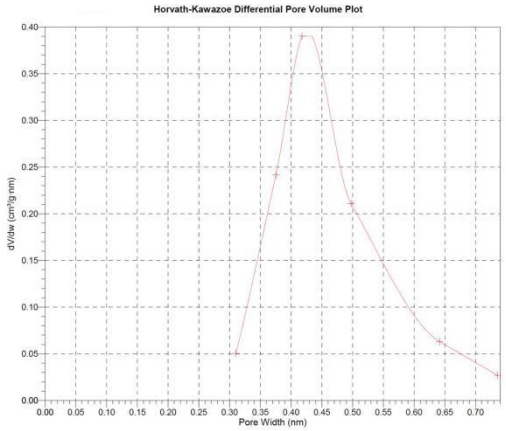

Figure 4. Nitrogen adsorption (+) and desorption (○) isotherm linear plot (a), the corresponding mesopore size distribution by BJH model (b), and the corresponding micropore size distribution by HK model (c) for the hard-carbon microspheres.

Table 2. The surface area, pore volume and pore size of the hard-carbon microspheres

Surface Area	BET Surface Area (m^2/g)	212.76
	t-Plot Micropore Area (m^2/g)	199.71
	BJH Adsorption cumulative surface area of pores between 1.7000 nm and 300.0000 nm diameter (m^2/g)	9.66
Pore Volume	DFT Total Volume in Pores <= 99.993 nm (cm^3/g)	0.084
	t-Plot micropore volume (cm^3/g)	0.077
	BJH Adsorption cumulative volume of pores between 1.7000 nm and 300.0000 nm diameter (cm^3/g)	0.014
Pore Size	Adsorption average pore width (4V/A by BET) (nm)	1.73
	Horvath-Kawazoe Median pore width (nm)	0.39
	BJH Adsorption average pore diameter (4V/A) (nm)	5.62

The surface area, pore volume and pore size of the hard-carbon microspheres are listed in Table 2. All of the above parameters that were calculated from N_2 adsorption isotherm showed an un-uniform pore structure. The PSD result indicated that the hard-carbon microspheres had more micropore structures than mesopore structures.

The BET specific area for the hard-carbon microspheres (212.76 $m^2 \cdot g^{-1}$) was much higher than the hard-carbon powder (5.29 $m^2 \cdot g^{-1}$). TAP data and yields of hard-carbon microspheres and the hard-carbon powder are also shown in Table 3. As well-known, the low tap density of hard-carbon powder is the main impediment to commercialization. The tap density of spherical hard-carbon is higher than the hard-carbon powder. By studying the yield step by step, it can be found that the yield difference between the two samples is due to the significant increase of low temperature solidification yield. During the

curing process for the microspheres, the loss of resin material was reduced due to the encapsulation effect of the microemulsion environment on the raw molecules.

Table 3. Physical property data and yields of the hard-carbon microspheres and the hard-carbon powder.

Samples	TAP $g \cdot cm^{-3}$	BET $m^2 \cdot g^{-1}$	Low temp. Solidification yield	Low temp. carbonization yield	High temp. carbonization yield	Total yield
Hard-carbon microspheres	0.9	212.76	92%	49%	92%	41.5%
Hard-carbon powder	0.7	5.29	72%	49%	92%	32.4%

3.2. Electrochemical performance of hard-carbon microsphere

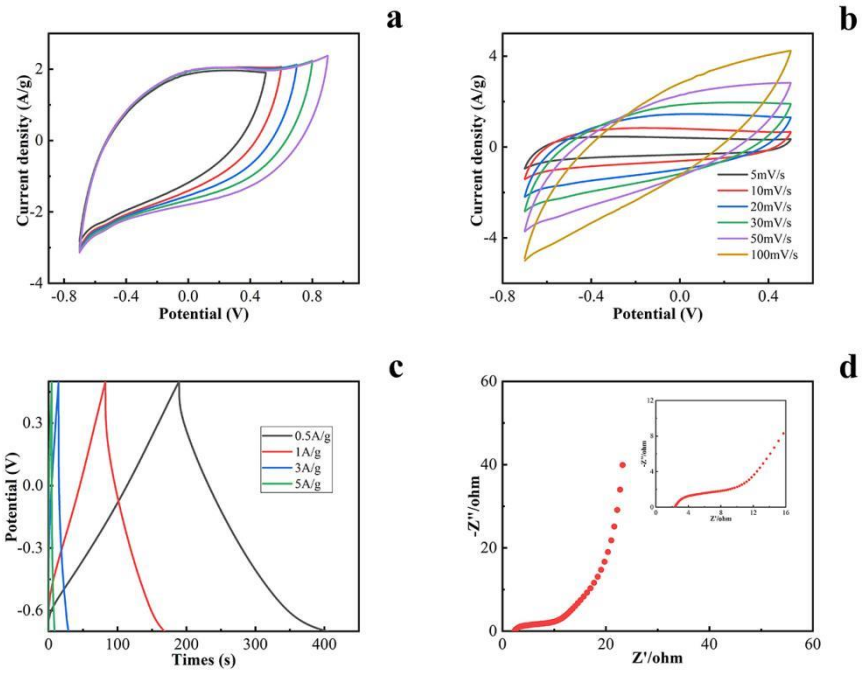

Figure 5. Electrochemical performance data of the hard-carbon microspheres as anode material in sodium ion capacitors: (a) The cyclic voltammetry (CV) curves at 30mV/s within different potential window ranges; (b) The CV curves at different sweep rates cycling between -0.7 and 0.5 V; (c) The galvanostatic charge–discharge (GCD) curves under different charge-discharge current densities; (d) The electrochemical impedance spectra (EIS) after tests

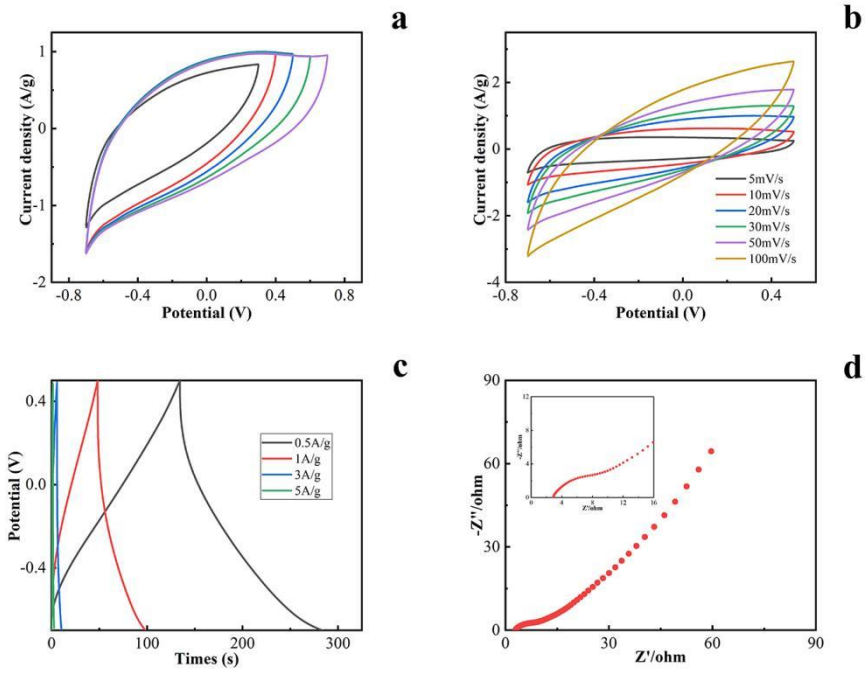

Figure 6. Electrochemical properties of the hard-carbon powder as anode material in sodium ion capacitors: (a) The CV curves at 30mV/s within different potential window ranges; (b) The CV curves at different sweep rates cycling between -0.7 and 0.5 V; (c) The GCD curves under different charge-discharge current densities; (d) The EIS data after tests

Lithium is a relatively low and expensive resource in the earth, therefore sodium-ion batteries with porous carbon as anode were developed, showing high energy density and power density [1]. Cyclic voltammograms and chronopotentiometric measurements have been used to evaluate the electrochemical properties of the as-prepared hard-carbon microspheres (Fig. 5) and the hard-carbon powder (Fig. 6) as anode materials in sodium ion capacitors. It can be seen that the suitable potential window was -0.7-0.5V at 30mV/s (Fig. 5a). As the electrode potential was widened from 0.3V to 0.5V, no obvious distortion of CV curve was observed. When the electrode potential exceeded 0.7V, the polarization phenomenon was obvious. The shape of the CV changed with increased scan rate (Fig. 5b and Fig. 6b), since the solution and electrode resistance can distort current response at the switching potential and this distortion is dependent upon the scan rate [31]. The GCD curves showed typical triangular shape, which also indicated that the electrodes had good electrochemical reversibility and high Coulomb efficiency (Fig. 5c). The equivalent series resistance (ESR) of the former electrode was 2.363Ω after measurement (Fig. 5d), while the latter was 2.890Ω (Fig. 6d). It revealed that the internal resistance of the former electrode was lower than the latter. The electrical conductivity for the hard-carbon microsphere was higher than the hard-carbon powder.

By comparison, it can be seen that the charge and discharge time for the hard-carbon microsphere electrode was longer (line a in Fig. 7a), and the electrode showed an approximate rectangular shape (line a in Fig. 7b), indicating that the hard-carbon microsphere electrode had an ideal electrochemical capacitance behavior. The hard-carbon powder electrode showed a spindle shape which was

distinguished from that of electric double-layer capacitance [32], in which case it was normally close to an ideal rectangular shape (line b in Fig. 7b). The area enclosed by CV line showed a decreased trend. The rate performance decreased significantly (line b in Fig.7c). Specific capacitance data for the hard-carbon as anode materials in sodium ion capacitors are listed in Table 4. Compared to the hard-carbon powder, the specific capacity for the hard-carbon microsphere increased and the rate performance increased obviously. The specific capacity for the hard-carbon microsphere electrode was 89.58 F g^{-1} when the current density was 0.5 A g^{-1}, and the electrode also had the best rate performance in sodium ion capacitors. The significant improvement of electrochemical performance can be attributed to the thermodynamic and kinetic factors that were influenced by the micropore structure and surface texture [33].

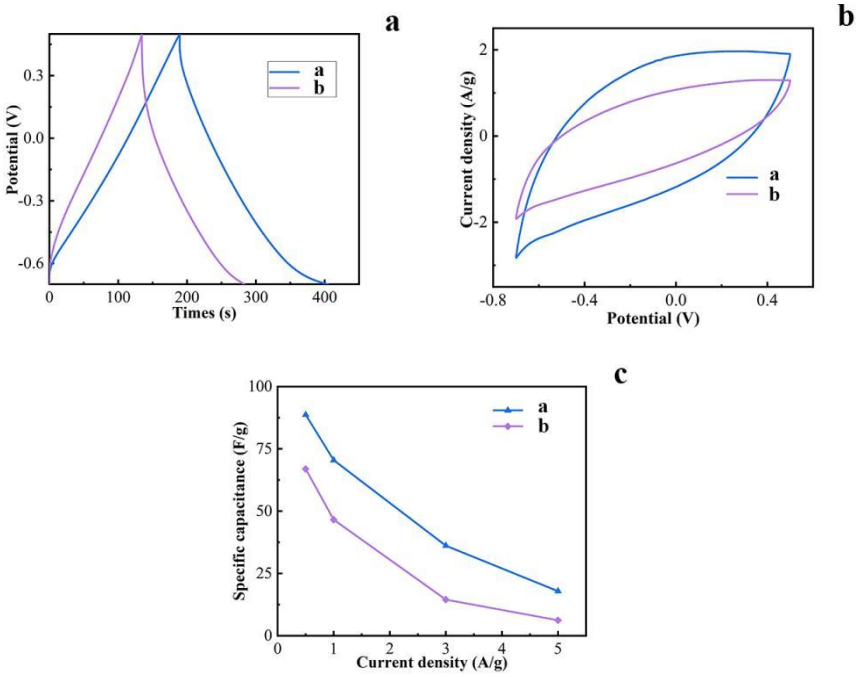

Figure 7. Electrochemical performance comparison diagrams of the hard-carbon microspheres (line a) and the hard-carbon powder (line b) as anode materials in sodium ion capacitors: (a) The charge–discharge curves under 0.5A/g; (b) The CV curves at 30mV/s between -0.7 and 0.5 V; (c) The rate performance

Table 4. Specific capacitance data of the hard-carbon microspheres (line a in Figure7a) and the hard-carbon powder (line b in Fig.7b) as anode materials in sodium ion capacitors

Samples	0.5A/g	1A/g	3A/g	5A/g
Hard-carbon microspheres (F/g)	89.58	71.50	35.75	17.08
Hard-carbon powder (F/g)	62.08	41.60	11.76	4.58

Table 5. Electrochemical performance data of the hard-carbon microspheres as anode material in lithium ion capacitors

Cathode active material	Internal resistance mΩ	Capacity F	Specific capacity $F \cdot g^{-1}$	Leak current mA	24h self discharge voltage V
Lithium iron phosphate (LFP)	27.80	199.09	309.44	0.88	4.07
Ternary material (NCM)	33.50	312.70	527.09	0.30	4.15

Electrochemical performance data for the hard-carbon microsphere as anode material are also obtained from the test results of button-type lithium ion capacitors listed in Table 5. These results showed that the Li storage for the hard-carbon microsphere in ternary material (NCM) system exhibited more excellent capacity performance than in Lithium iron phosphate (LFP) system. The hard-carbon microsphere delivered a high reversible specific capacity of 527.09 F g^{-1} for NCM system and 309.44 F g^{-1} for LFP system, respectively. It is reported that the hybrid Li-metal and Li-ion storage mechanism for hard-carbon anode material is consist of a Li-metal surface absorption followed by the intercalation of Li-ions [34]. In view of potential application, hard carbon materials could be used for high power-density capacitors by limiting the voltage range to permit only the Li-intercalation reaction [28]. As for sodium ion capacitors with low cost and safety, further optimization of the micropore structure and surface texture for the hard-carbon material should be considered.

4. CONCLUSIONS

Hard-carbon microspheres were synthesized by the microemulsion-mediated hydrothermal method, while hard-carbon powder was prepared by the normal hydrothermal method for comparison. Results from nitrogen adsorption isotherm indicated that the hard-carbon microsphere material had narrower particle size distribution and more uniform dispersion. The electrical conductivity and rate performance for the hard-carbon microsphere anode increased obviously in sodium ion capacitors. The specific capacity of the hard-carbon microsphere electrode was 89.58 F g^{-1} at 0.5 A g^{-1}. Besides, the hard-carbon microsphere anode had Li-storage specific capacity of 309.44 and 527.09 $F \cdot g^{-1}$ in LFP and NCM system, respectively. In view of potential application, the hard-carbon microsphere could be appropriate candidate anode material for high power-density Na-ion and Li-ion capacitors.

References

1. N.-S. Choi, Z. Chen, S.A. Freunberger, X. Ji, Y.-K. Sun, K. Amine, G. Yushin, L.F. Nazar, J. Cho and P.G. Bruce, *Angew. Chem. Int. Ed*., 51 (2012) 9994.

2. S. Zhang, L. Sui, H. Dong, W. He, L. Dong and L. Yu, *ACS Appl. Mater. Interfaces*, 10 (2018) 12983.
3. W. Li, L. Zhou and W. Liao, *Int. J. Electrochem. Sci.*, 16 (2021) Article ID: 211013, doi: 10.20964/2021.10.04.
4. H. Shi, J. Barker, M.Y. Saidi and R. Kosbang, *J. Electrochem. Soc*., 28 (1997) 3466.
5. J.R. Dahn, T. Zheng, Y. Liu and J.S. Xue, *Chem. Mater.*, 8 (1996) 389.
6. T. Zheng, W. Xing and J.R. Dahn, *Carbon,* 34 (1996) 1501.
7. O. Kwon, Y. Jung, J. Kim and S.M. Oh, *J. Power Sources*, 125 (2004) 221.
8. J. Lee, H. Lee, S. Oh, S. Lee, K. Lee and S. Lee, *J. Power Sources*, 166 (2007) 250.
9. G. Fey, D.C. Lee and Y.Y. Lin, *J. Power Sources*, 119 (2003) 39.
10. K. Sato, M. Noguchi, A. Demachi, N. Oki and M. Endo, *Science*, 264 (1994) 556.
11. X. Zhang, S. Han, C. Fan, L. Li and W. Zhang, *J. Solid State Electrochem.*, 19 (2014) 715.
12. M. Tang, D. Zhao, J. Li, P. Li, J. Duan, R. Wang, J. Teng and C. Yuan, *Int. J. Electrochem. Sci.*, 16 (2021) Article ID: 210432, doi: 10.20964/2021.04.57.
13. R. Yang, X. Qiu, H. Zhang, X. Huang and L. Chen., *Carbon*, 43 (2005) 11.
14. L. Pei, L. Yang and H. Cao, *Electrochim. Acta*, 364 (2020) 137313.
15. Z. Ma, X. Yuan, D. Li, X. Liao, H. Hu, J. Ma and J. Wang, *Electrochem. Commun*., 4 (2002) 188.
16. J. Wang, W. Lv, Q. Ren, L. Yan and Z. Shi, *Appl. Surf. Sci*., 558 (2021) 149824.
17. J. Xie, G.S. Cao and X.B. Zhao, *Mater. Chem. Phys*., 88 (2004) 295.
18. G.X. Wang, J. Yao, H.K. Liu, S.X. Dou and J. Ahn, *Electrochim. Acta*, 50 (2004) 517.
19. Q. Wang, H. Li, L. Chen and X. Huang, *Carbon*, 39 (2001) 2211.
20. J. Jiang, Y. Zhang, Z. Li, Y. An, Q. Zhu, Y. Xu, S. Zang, H. Dou and X. Zhang, *J. Colloid Interface Sci*., 567 (2020) 75.
21. Nagmani and S. Puravankara, *ACS Appl. Energy Mater.*, 3 (2020) 10045.
22. K. Yu, Y. Wang, X. Wang, W. Liu, J. Liang and C. Liang, *Mater. Lett.*, 253 (2019) 405.
23. Z. Zou and C. Jiang, *J. Mater. Sci. Technol.*, 35(2019) 644.
24. Y. Wu, C. Wan, C. Jiang, S. Fang and Y. Jiang, *Carbon*, 37 (1999) 1901.
25. L. Wang, Y. Zhang and M. Muhammed, *J. Mater. Chem*., 5 (1995) 309.
26. V. Chhabra, V. Pillai, B.K. Mishra, A. Morrone and D.O. Shah, *Langmuir*, 11 (1995) 3307.
27. M. Wu, J. Long, A. Huang, Y. Luo, S. Feng and R. Xu, *Langmuir,* 15 (1999) 8822.
28. J. Hu, H. Li and X. Huang, *Solid State Ionics*, 176 (2005) 1151.
29. D. Zhao, W. Zhou and H. Li., *Chem. Mater.*, 19 (2007) 3882.
30. Y.F. Du, G.H. Sun, Y. Li, J.Y. Cheng, J.P. Chen, G. Song, Q.Q. Kong, L.J. Xie and C.M. Chen, *Carbon*, 178 (2021) 243.
31. J.H. Jiang and A. Kucernak, *Electrochim. Acta*, 47 (2002) 2381.
32. D.-D. Zhao, M.W. Xu, W.-J. Zhou, J. Zhang and H.L. Li., *Electrochim. Acta*, 53 (2008) 2699.
33. J.Z. Hou, X.Y. Mao, J.Y. Wang, C. Liang and J.C. Liang, *Chem. Phys.*, 551 (2021) 111352.
34. K. Wang, Y. Xu, H. Wu, R.L. Yuan, M. Zong, Y. Li, V. Dravid, W. Ai and J.S. Wu, *Carbon*, 178 (2020) 443.